J. Fluid Mech. (2015), *vol.* 766, *pp.* 129–146.
doi:10.1017/jfm.2015.11

Ultrasonic atomization of liquids in drop-chain acoustic fountains

Julianna C. Simon[1,†], Oleg A. Sapozhnikov[1,2], Vera A. Khokhlova[1,2], Lawrence A. Crum[1] and Michael R. Bailey[1]

[1]Center for Industrial and Medical Ultrasound, Applied Physics Laboratory, University of Washington, Seattle, WA 98105, USA

[2]Department of Acoustics, Physics Faculty, Moscow State University, Moscow, 119991, Russian Federation

(Received 13 March 2014; revised 29 August 2014; accepted 6 January 2015; first published online 2 February 2015)

When focused ultrasound waves of moderate intensity in liquid encounter an air interface, a chain of drops emerges from the liquid surface to form what is known as a drop-chain fountain. Atomization, or the emission of micro-droplets, occurs when the acoustic intensity exceeds a liquid-dependent threshold. While the cavitation-wave hypothesis, which states that atomization arises from a combination of capillary-wave instabilities and cavitation bubble oscillations, is currently the most accepted theory of atomization, more data on the roles of cavitation, capillary waves, and even heat deposition or boiling would be valuable. In this paper, we experimentally test whether bubbles are a significant mechanism of atomization in drop-chain fountains. High-speed photography was used to observe the formation and atomization of drop-chain fountains composed of water and other liquids. For a range of ultrasonic frequencies and liquid sound speeds, it was found that the drop diameters approximately equalled the ultrasonic wavelengths. When water was exchanged for other liquids, it was observed that the atomization threshold increased with shear viscosity. Upon heating water, it was found that the time to commence atomization decreased with increasing temperature. Finally, water was atomized in an overpressure chamber where it was found that atomization was significantly diminished when the static pressure was increased. These results indicate that bubbles, generated by either acoustic cavitation or boiling, contribute significantly to atomization in the drop-chain fountain.

Key words: acoustics, aerosols/atomization, drops and bubbles

1. Introduction

Ultrasonic atomization, or the emission of a fog of micro-droplets from an acoustically excited liquid–air interface, has been well-known since the landmark experiment by Wood & Loomis (1927). Since then, ultrasonic atomization has been used commercially in air humidifiers, medical nebulizers, and other such devices. However, the mechanism of atomization is still not well understood. Currently, the

† Email address for correspondence: jcsimon@uw.edu

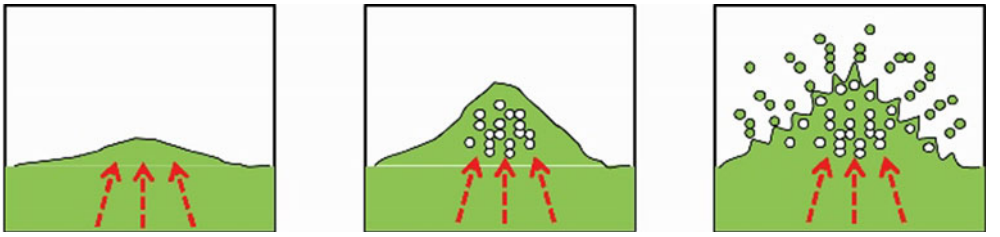

FIGURE 1. (Colour online) Schematic depicting the cavitation-wave hypothesis describing atomization from a focused ultrasound wave encountering a liquid–air interface. The focused wave forms a protuberance in the liquid surface, focusing the wave inverted from the pressure-release interface and causing cavitation bubbles to form within the liquid protuberance. Oscillations of the cavitation bubbles along with capillary waves on the liquid surface facilitate the pinch-off of droplets in atomization.

most accepted theory of atomization is the cavitation-wave hypothesis (illustrated in figure 1), which states that a combination of capillary waves on the liquid surface (i.e. Faraday ripples) along with acoustically driven bubble oscillations beneath the liquid surface (i.e. acoustic cavitation) cause the droplets to be emitted (Rozenberg 1973). Further, the surface is often transformed into a fountain in the shape of a stack or chain of nearly spherical drops, and any one drop in the chain can atomize, presumably by a similar process. There remains debate as to the relative contributions of bubbles and surface instabilities, particularly in the drop-chain fountain. In this paper, high-speed videography of water atomization at different frequencies, temperatures, and static pressure levels, as well as the atomization of other liquids, is used to provide experimental evidence as to the mechanism of atomization, specifically in the regime when a focused ultrasound beam creates an acoustic fountain in the form of a drop chain. We hypothesize that bubbles are a significant mechanism of liquid atomization in the drop-chain fountain.

Previously, researchers have investigated the role of cavitation in liquid atomization with sonoluminescence and the manipulation of material surface tension, shear viscosity, and ambient pressure (Sollner 1936; Rozenberg & Eknadiosyants 1960; Gershenzon & Eknadiosyants 1964; Il'in & Eknadiosyants 1967, 1969). Many of the initial studies were conducted using plane-wave ultrasound with frequencies ranging between 10 kHz and 1.5 MHz (Wood & Loomis 1927; Antonevich 1959; Lang 1962; Boguslavskii & Eknadiosyants 1969; Topp 1973; Barreras, Amaveda & Lozano 2002). Results from these studies were unclear as to whether atomization from the plane wave arose from parametric instabilities (i.e. capillary waves) or from cavitation bubble oscillations. More recently, the mechanism of plane-wave atomization for the specific case of thin-film surface acoustic-wave nebulization was investigated, where it was found that atomization was a result of capillary-wave breakup rather than cavitation (Qi, Yeo & Friend 2008; Collins *et al.* 2012; Blamey, Yeo & Friend 2013). When the plane ultrasound wave was replaced with focused waves in the megahertz frequency range (0.5–5.4 MHz), it was found that atomization arose from a liquid fountain (McCubbin 1953; Gershenzon & Eknadiosyants 1964; Eknadiosyants 1968; Boguslavskii & Eknadiosyants 1969; Bassett & Bright 1976). At moderate acoustic intensities, the fountain took the form of a chain of drops on the order of millimetres in diameter, and atomization arose from the drops in the chain. At higher acoustic intensities, the fountain was less defined and atomization ensued from a liquid

protuberance similar to what is illustrated in figure 1 (Simon *et al.* 2012). The figure depicts one version of the cavitation-wave hypothesis for a focused ultrasound wave which begins with the radiation force from the focused wave causing a protuberance to form in the liquid surface. When the protuberance forms, coherent interaction between the waves incident on and reflected from the pressure-release interface results in the formation of numerous cavitation bubbles within the protuberance. Acoustic emissions from the oscillation and collapse of these cavitation bubbles separately or synergistically add to the surface ripples caused by capillary-wave instabilities and facilitate the pinch-off of droplets in atomization. Besides proposing that atomization is the result of capillary waves and cavitation bubbles, some iterations of the cavitation-wave hypothesis also suggest that the size of the emitted droplets depends upon the mechanism of release: capillary-wave instabilities emit small, consistent-sized micro-droplets while cavitation bubble oscillations and collapses emit larger, more diverse-sized micro-droplets (Antonevich 1959). While many of the experimental results, especially those from a focused source, support some version of the cavitation-wave hypothesis, there is still some debate as to the mechanism, or relative contributions of a variety of mechanisms, of atomization particularly in the drop-chain fountain.

In the decades since the initial atomization studies, high-speed photography technologies have improved significantly, allowing more precise observations of atomization. Recently, we showed that atomization from the top drop in a drop-chain fountain at 2.165 MHz could arise in less than 100 μs from a triangular-shaped distortion (Simon *et al.* 2012). These observations of atomization along with the video frames published in Rozenberg (1973) led to several hypotheses of atomization specific to drop-chain fountains that were detailed in Simon *et al.* (2012). The first possibility was that the top drop in the chain becomes a spherical acoustic resonator, in which highly excited radial oscillations at some stage become unstable causing non-spherical shape deformations that break the drop into pieces. The second possible mechanism was that a cavitation bubble (or bubble cloud) forms in the centre of the drop (where the standing pressure wave amplitude is at its maximum) causing the liquid to move unchecked from the centre of the drop. The final hypothesis was boiling: shocks could form while the spherical wave is reverberating in the drop and cause localized heat deposition near the drop centre, and when the temperature reaches or exceeds 100 °C (providing for some superheating in the absence of a suitable nucleus), a vapour bubble forms and the drop explodes. The first two suggested mechanisms are captured in the cavitation-wave hypothesis; however, the novel idea presented here is that heat deposition and boiling could contribute to atomization in the drop-chain fountain.

The goal of this paper is to provide experimental evidence that bubbles are a significant driving force for atomization in drop-chain fountains. High-speed photographic images of atomization are reported encompassing a range of ultrasonic frequencies and for liquids of various viscosities, surface tensions, and boiling points. In addition, images of water atomization in an overpressure chamber at static pressure levels up to 14 MPa are also presented and described. The experimental descriptions of atomization in drop-chain fountains enhance the understanding of the basic physical phenomena and provide the basis for future numerical modelling.

2. Methods

2.1. *Effect of frequency on atomization*

Three different focused ultrasound transducers were operated at frequencies of 2.165 MHz, 1.04 MHz, and 155 kHz to determine the effect of frequency on

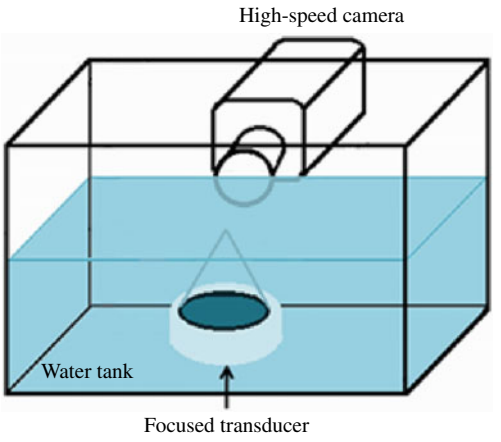

FIGURE 2. (Colour online) Experimental arrangement for water atomization. Exposures were recorded with a high-speed camera and backlit (not shown).

atomization of water in a drop-chain fountain. All three transducers were air-backed, single-element, piezoceramic crystals (PZ 26, Ferroperm Piezoceramics, Kvistgaard, Denmark) with spherical bowl shapes and were mounted in custom-built polycarbonate housings. The F-number (i.e. the ratio between the focal length and source diameter) was one ($F = 1$) for all three transducers: both the 2.165 and 1.04 MHz transducers had aperture diameters and radii of curvature of 45 mm; the 155 kHz transducer had a larger, 100 mm aperture diameter and radius of curvature. A function generator (Model 33250A, Agilent, Palo Alto, CA, USA) and linear radiofrequency amplifier (55 dB, model A300, ENI, Rochester, NY, USA) were used to drive the transducers.

The transducers were focused at the surface of filtered, degassed water, and the acoustic fountain was recorded with a Photron APX-RS high-speed camera (monochrome, Photron, San Diego, CA) as shown in figure 2. Videos taken at 5000–30 000 frames per second (f.p.s.) were backlit with a flash or continuous disperse light source (Photogenic PowerLight 2500DR, Bartlett, IL, USA). A Carl Zeiss lens (Makro-Planar T*2/100, Thornwood, NY, USA) with a bellows extension provided a resolution on the order of 40 μm pixel^{-1}.

Prior to experimentation, the 2.165 and 1.04 MHz transducers were characterized using a fibre-optic probe hydrophone (FOPH 2000, RP Acoustics, Leutenbach, Germany) with a 100 μm active diameter. The acoustic field produced by the 155 kHz transducer was mapped with a calibrated Onda Reson hydrophone (Onda Corporation, Sunnyvale, CA, USA) at low input voltages and scaled to the voltages used for atomization. As all transducers were operated at or near the linear regime, the measured waveforms were nearly sinusoidal and are not shown here.

2.2. *Heated water atomization*

To test the hypothesis that boiling could explain atomization in the drop-chain fountain, an experiment was conducted where water was heated to approximately 60 °C and atomized regularly while cooling. The same 2.165 MHz transducer that was described previously was used in the experimental configuration shown in figure 2. After stirring the solution to minimize local temperature gradients, a thermocouple was used to measure the bulk water temperature for each exposure. Water was atomized

	ρ (kg m^{-3})	c (m s^{-1})	α (dB cm^{-1})	b.p. (°C)	η (mPa s)	σ (mN m^{-1})
Water	998	1486	0.0022	100	0.9	72.8
Ethanol	785	1144	0.0044	78	1	22
Castor oil	969	1452	0.4600	313	990	35.1
Glycerol	1260	1904	0.2600	290	1200	64
n-propanol	803	1205	0.0058	97	1.96	24
Olive oil	915	1440	0.1200	300	84	36
1,3-butanediol	1005	1530	0.1100	204	97	37

TABLE 1. Properties of liquids used at 25 °C and atmospheric pressure: $\rho =$ density; $c =$ sound speed; $\alpha =$ acoustic absorption coefficient at 1 MHz; b.p. = boiling point; $\eta =$ shear viscosity; $\sigma =$ surface tension (Treeby *et al.* 2009; Kujawska 2012; Maxwell *et al.* 2013; National Physical Laboratories 2013; The Engineering Toolbox 2013).

at a focal acoustic intensity of 180 W cm^{-2}. This intensity level was chosen because it was shown to be the level at which atomization first appeared (inconsistently) at 20 °C (Simon *et al.* 2012). The time for atomization to commence (after turning on the ultrasound source) was determined from recorded high-speed videos and plotted versus temperature to determine whether a relationship exists between the liquid temperature and its atomization.

2.3. *Atomization of other liquids*

Even though shear viscosity is known to affect all three proposed mechanisms of atomization (capillary waves, acoustic cavitation, and boiling), liquids of various shear viscosities were investigated to test whether atomization ceased when the shear viscosity was increased. Previously, atomization was attempted in glycerol, castor oil, and 70 % ethanol (Simon *et al.* 2012); other liquids, including olive oil, 1,3-butanediol, and *n*-propanol were also tested. In particular, olive oil and 1,3-butanediol were included because they had similar sound speeds and densities to water, but significantly higher boiling temperatures. Additionally, a recent paper by Maxwell *et al.* (2013) showed that the cavitation threshold negative pressure amplitude for a single cycle of focused ultrasound in olive oil and 1,3-butanediol was greater than 35 MPa whereas the cavitation threshold for distilled and degassed water was measured to be $p_- = 27.4$ MPa (peak negative pressure). The other chemical, *n*-propanol, was of interest because it has a boiling point similar to that of water but double the shear viscosity. The physical properties of these liquids are listed in table 1.

The same 2.165 MHz transducer was used that was described previously. The liquids were poured with variable thicknesses between 2 and 10 mm into a custom-designed container with an acoustically transparent, thin-film bottom. The container was partially submerged in a water tank to couple the liquid in the container to the focused transducer while maintaining a free liquid–air interface. As before, atomization events were monitored using high-speed videography and the transducer was driven with the same function generator and radiofrequency amplifier as described previously. Reported intensities include both the water measurement and the intensity derated through the thin liquid layer by multiplying the level measured in water with the factor $\exp(-2(\alpha - \alpha_0)h)$, where α is the acoustic absorption coefficient

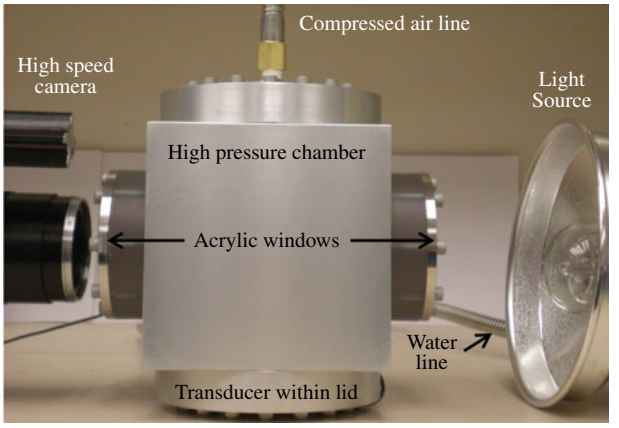

FIGURE 3. (Colour online) Photograph of the experimental configuration for high static pressure atomization. Exposures were recorded through acrylic windows on either side of the chamber. Overpressure was induced using a compressed air cylinder controlled by a regulator. The transducer was built into the lower lid of the chamber and was a flat, piezoceramic source that was focused by a curved, aluminium lens and operated at 2.127 MHz.

of the liquid (see table 1), α_0 is the absorption coefficient of water, and h is the liquid layer thickness. The absorption coefficient was assumed to grow quadratically with frequency (i.e. $\alpha(f) = \alpha_0 f^2$) except in the cases of castor oil and olive oil, which were previously shown to have 1.67 power dependences on frequency (Treeby *et al.* 2009; Kujawska 2012).

2.4. *High static pressure atomization*

Increasing the static pressure has been shown to suppress bubble activity for other ultrasound-based applications (Bronskaya *et al.* 1968; Hill 1971; Bailey *et al.* 2001; Sapozhnikov *et al.* 2002; Khokhlova *et al.* 2006). To separate the effects of bubbles, either acoustic cavitation or boiling, from surface instabilities in atomization of the drop-chain fountain, overpressure was applied to a pressure chamber containing a water–air interface. The aluminium-walled overpressure chamber with acrylic windows is shown in figure 3. A 2.127 MHz transducer was built into the bottom lid of the chamber using a flat, 40 mm, piezoceramic source that was focused at the water surface using an aluminium lens. Before experimentation, the waveforms of the aluminium-lensed transducer were measured with the same fibre-optic probe hydrophone that was described previously. As atomization requires a pressure-release (or liquid–air) interface, overpressure was induced using compressed air and controlled with a regulator (ProStar 4092, Praxair, Seattle, WA, USA). Water level within the chamber was controlled by a hydraulic syringe pump, which allowed the water level to be manipulated even when the chamber was pressurized. The acrylic windows in the sides of the chambers allowed recording with the same Photron high-speed camera and backlighting with the same Photogenic continuous light source that were described previously, but with a slightly better resolution on the order of 20 μm pixel^{-1}.

With the exception of the heated-water atomization experiment (which was only repeated for a different intensity), all of these experiments were repeated several times. While only a few sample images are presented and discussed in detail, the trends were replicated and are representative of images taken under similar conditions.

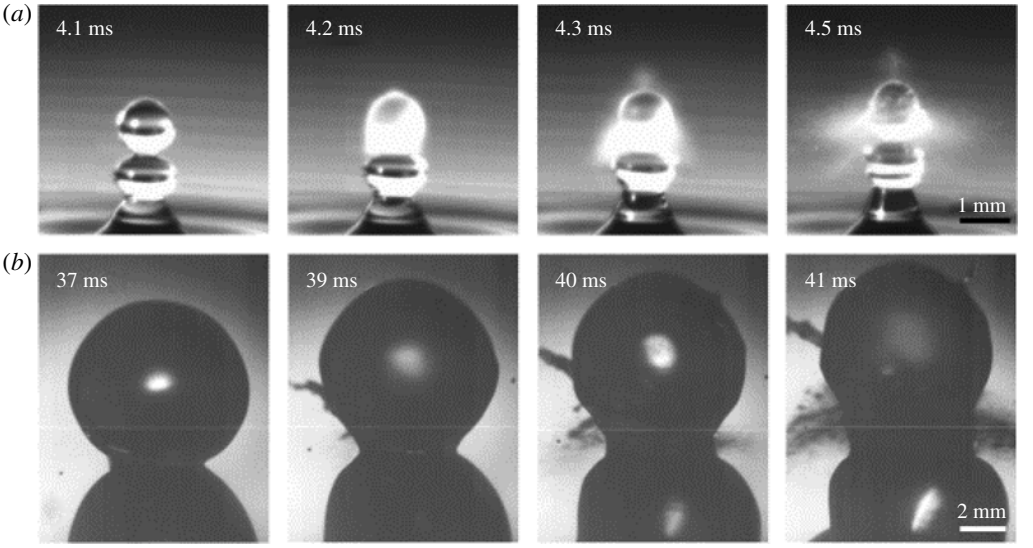

FIGURE 4. (*a*) Water atomization from a 1.04 MHz focused ultrasound transducer operating at 245 W cm^{-2} ($p_+ = 3.1$ MPa and $p_- = 2.3$ MPa) and recorded at 30 000 f.p.s. The water drops in the chain oscillate around 1.5 mm in diameter. The top drop changes from transparent to opaque in less than 0.1 ms and begins to explode outward in a triangular pattern with jet velocities up to 15 m s^{-1}. (*b*) Water atomization from a 155 kHz focused ultrasound transducer operating at 264 W cm^{-2} ($p_+ = p_- = 2.8$ MPa) and recorded at 5000 f.p.s. The water drops in the chain oscillate around 7.5 mm in diameter, and the jets explode outward from the neck region between the drops in the chain at velocities of 2–4 m s^{-1}. Supplementary movie 1 shows this figure in video format, available online at http://dx.doi.org/10.1017/jfm.2015.11.

3. Results

3.1. *Effect of frequency on atomization*

For all frequencies tested, a drop-chain fountain forms at low acoustic intensities without atomization. As the acoustic intensity increases, atomization arises from the drop-chain fountain, generally from the top drop in the chain; we define the threshold intensity to be the acoustic intensity at which atomization occurs consistently within a 10 ms pulse. When the acoustic intensity is further elevated, the drop-chain fountain structure becomes less defined and atomization increases. At an ultrasonic frequency of 1.04 MHz and a focal threshold intensity of 245 W cm^{-2} as shown in figure 4(*a*), droplets on the order of tens of microns in diameter (limited by camera resolution) are emitted in a triangular (or possibly conical) pattern at horizontal velocities of approximately 15 m s^{-1} and vertical velocities of 7 m s^{-1}. Before atomization commences, the top drop in the chain changes from transparent to opaque in less than 33 μs, the temporal resolution of the video. The diameter of the drops in the drop-chain fountain oscillates around 1.5 mm, which is approximately equal to the wavelength of the 1.04 MHz transducer (1.43 mm). The entire droplet explosion sequence occurs in less than 1 ms.

When the frequency is decreased to 155 kHz, the top drop in the chain atomizes when exposed to a threshold intensity of 264 W cm^{-2} as shown in figure 4(*b*). The mean diameter of the drop chain is 7.5 mm, which is somewhat smaller than

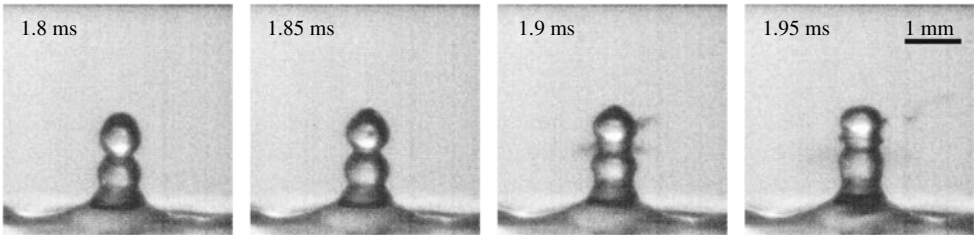

FIGURE 5. Water atomization from a 2.165 MHz focused transducer operating at 180 W cm^{-2} ($p_+ = 2.5$ MPa, $p_- = 2$ MPa) and recorded at 20 000 f.p.s. with diffuse lighting. In the second frame, there is a shadow just to the right of centre in the top drop of the chain, which we speculate to be a bubble (or bubble cloud). In the next frame, taken 0.05 ms later, jets of droplets are released from the top drop in the drop-chain fountain. This figure is included in video format in supplementary movie 1.

(but approximately equal to) the calculated acoustic wavelength in water at 155 kHz (9.59 mm). The emitted droplets range from tens of microns (limited by camera resolution) up to 600 μm in diameter and are emitted at velocities of 2–4 m s^{-1}. Compared to atomization at 1.04 MHz, atomization at 155 kHz takes ten times as long to commence (4.1 ± 0.4 ms at 1.04 MHz compared to 34 ± 2 ms at 155 kHz). This corresponds to approximately 4200 cycles for atomization to commence at 1.04 MHz or 5300 cycles for atomization to commence at 155 kHz.

In an effort to visualize bubbles in the drop-chain fountain, the lighting was changed from direct backlighting by adding a diffuser, and the camera depth of focus was decreased. The water–air interface was exposed to 2.165 MHz ultrasound operating at 180 W cm^{-2} (an intensity at which atomization occurred inconsistently) and recorded at 20 000 f.p.s. as shown in figure 5. The mean diameter of the drop chain is 0.62 mm, which is approximately equal to the calculated wavelength at 2.165 MHz (0.69 mm). As shown in the centre frames of figure 5, a shadow appears to the right of centre in the top drop of the chain immediately before an atomization event occurs; the atomized droplets are emitted at velocities up to 16 m s^{-1}. While the shadow in the top drop is not observed every time before atomization, when it is present it is always immediately followed by the release of atomized droplets. We posit that the shadow is caused by a bubble (or bubble cloud) in the drop. This speculation is supported by work from Tomita & Tanaka (2012) who observed cavitation activity in the top drop of the drop-chain fountain prior to atomization. The results for atomization at the three different frequencies are summarized in table 2; the atomized droplet velocity is included for comparison to the calculated particle velocity of the incident wave for each frequency/intensity pair, which depends on the focal acoustic pressure, liquid density, and liquid speed of sound.

3.2. *Heated water atomization*

The effect of temperature on atomization in the drop-chain fountain was investigated and the time to the initial atomization event versus bulk water temperature is plotted in figure 6. A general trend is apparent in that as the temperature increases, the time to the commencing of atomization decreases. In three cases, which are marked at 10 ms with an open diamond for the measured temperature, atomization did not occur within the 10 ms pulse. This was unsurprising as at 20 °C, atomization occurs inconsistently at the 180 W cm^{-2} intensity.

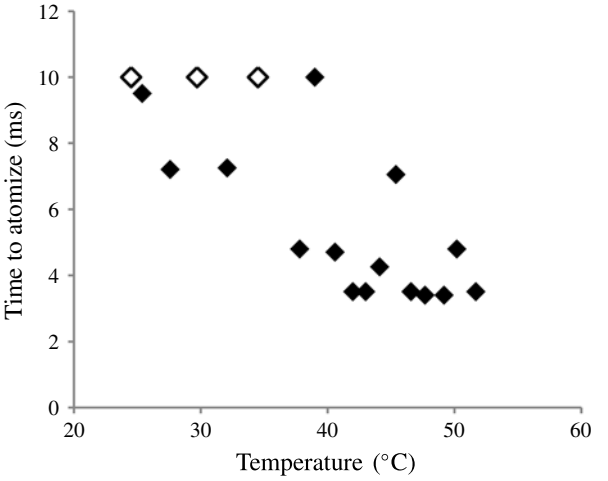

FIGURE 6. Plot showing the time to commence atomization versus bulk water temperature. The three open diamonds located at 10 ms indicate that atomization did not occur at the measured temperature within the 10 ms pulse. All other data show an approximate trend: as the temperature increases, the time to commence atomization decreases.

Frequency	Intensity (W cm^{-2})	Acoustic wavelength (calculated) (mm)	Drop-chain diameter (observed) (mm)	Atomized droplet velocity (observed) (m s^{-1})	Particle velocity of the incident wave (calculated) (m s^{-1})
2.165 MHz	180	0.69	0.62	11–16	1.68
1.04 MHz	245	1.43	1.5	7–15	2.09
155 kHz	264	9.59	7.5	2–4	1.88

TABLE 2. Comparison between calculations and observations for three frequencies at 25 °C.

3.3. *Atomization of other liquids*

When water is exchanged for 70 % ethanol (as shown in figure 7*a*), a few relatively large droplets (approximately 200 μm in diameter) are emitted at velocities of 2–4 m s^{-1} upon exposure to 2.165 MHz ultrasound at the atomization threshold intensity of 180 W cm^{-2}. The mean diameter of the drops in the drop-chain fountain for 70 % ethanol is smaller (0.59 mm) than was observed previously in water at 2.165 MHz (0.62 mm). Note that this fact is in accordance with the lower sound speed in ethanol (1144 versus 1486 m s^{-1}); the calculated drop diameter in ethanol at 2.165 MHz is 0.53 mm. Castor oil and glycerol form fountains but do not atomize when exposed to 2.165-MHz ultrasound at the maximum acoustic intensity in water of 24 000 W cm^{-2} (shown in figure 7*b,c*), even for very thin (approximately 2 mm thick) layers (derated intensities are 12 000 W cm^{-2} and 15 000 W cm^{-2} for castor oil and glycerol, respectively). The mean diameter of the glycerol drop-chain fountain is 0.79 mm (calculated wavelength is 0.88 mm) and propagates vertically at 2 m s^{-1}. In castor oil, the sides of the fountain are smooth with no drop-chain structure; the fountain propagates vertically at 2.4 m s^{-1} with a consistent diameter of 0.83 mm (calculated wavelength is 0.68 mm).

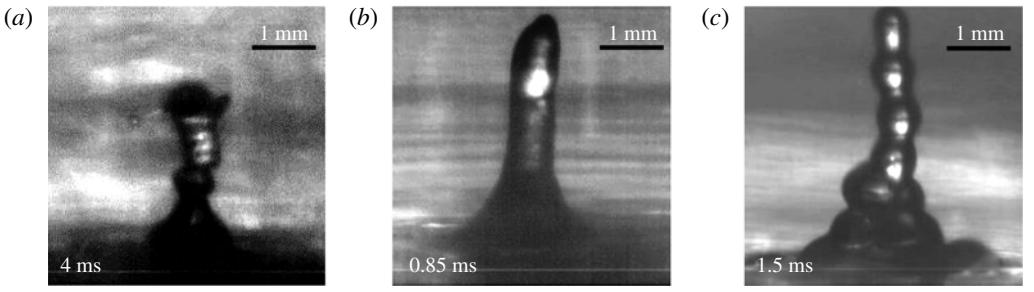

FIGURE 7. (*a*) Atomization of 70 % ethanol when exposed to 2.165 MHz focused ultrasound at 180 W cm^{-2}. The emitted droplets (one visible in the photo just to the left of the drop chain) are larger and emitted more slowly than atomization of water for a similar frequency and intensity. Both (*b*) castor oil, and (*c*) glycerol do not atomize, even when exposed to 2.165 MHz ultrasound at the maximum intensity (in water) of 24 000 W cm^{-2} ($p_+ = 65$, $p_- = 16$ MPa).

When water is exchanged for olive oil or 1,3-butanediol, jets (as opposed to discrete droplets) are released that appear qualitatively different from those of water. Figure 8(*a*) shows olive oil atomization at the derated threshold intensity of 240 W cm^{-2} (550 W cm^{-2} in water). Thin jets are emitted that remain partially connected to the olive oil drop-chain fountain before eventually being released as a discrete droplet. Atomization of 1,3-butanediol occurs similarly, although the derated atomization threshold of 1,3-butanediol is higher at 360 W cm^{-2} (not shown). Jets released from either olive oil or 1,3-butanediol have similar diameters of approximately 70 μm and reach velocities up to 7 m s^{-1}. The mean diameter in the olive oil drop-chain fountain is 0.64 mm (calculated wavelength is 0.67 mm).

Atomization exposures were also conducted in *n*-propanol, a chemical that has a similar boiling point to water but double the shear viscosity. Figure 8(*b*) shows *n*-propanol atomization at the derated intensity of 350 W cm^{-2} (365 W cm^{-2} in water), an intensity above the atomization threshold of *n*-propanol of 180 W cm^{-2}. The droplets explode outward in a triangular pattern at velocities up to 10 m s^{-1}. The initial triangular atomization event excites more atomization events past the 1 ms time point (not shown). Except for the jet connected to the upper surface of the drop-chain fountain, individual droplets are emitted with diameters on the order of tens of microns (measurement precision limited by camera resolution). The mean diameter of the *n*-propanol drop-chain fountain is 0.58 mm (calculated wavelength is 0.55 mm).

3.4. *High static pressure atomization*

As the transducer in the high static pressure chamber differs in design from those used previously (aluminium-lensed focusing as compared to curved piezoceramic focusing), the intensity at which water begins to atomize (albeit inconsistently) at 2.127 MHz of 200 W cm^{-2} ($p_+ = 2.5$ MPa, $p_- = 2.4$ MPa), was compared and found to be similar to the intensity for inconsistent water atomization of 180 W cm^{-2} reported in a previous study (Simon *et al.* 2012). When water is exposed to 850 W cm^{-2} (shown in figure 9), atomization is very dramatic at atmospheric pressure (0.1 MPa) with many droplets released from a vaguely drop-chain-like fountain with diameters of less than 20 μm (1 pixel) to 400 μm and velocities up to 8 m s^{-1}. Yet when the

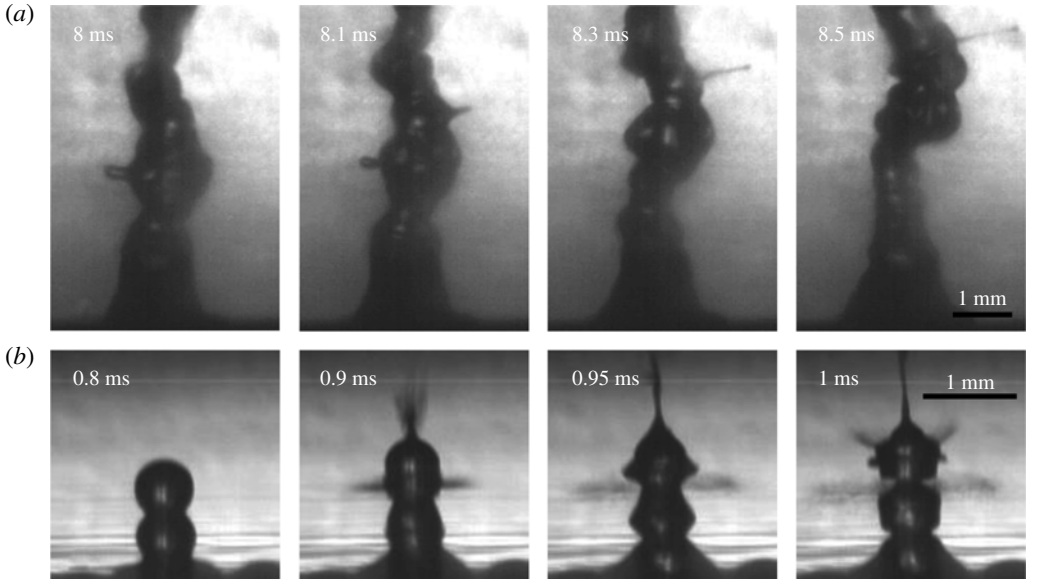

FIGURE 8. (*a*) Olive oil atomization from 2.165 MHz focused ultrasound operating at an intensity (in water) of 550 W cm^{-2} ($p_+ = 5.5$ MPa, $p_- = 4$ MPa). A jet begins to be emitted from the left-hand side of the drop chain, but collapses rather than being ejected from the chain. On the right-hand side of the drop chain, a 70 μm diameter jet is emitted with a velocity of 3.7 m s^{-1}. (*b*) *n*-propanol atomization from 2.165 MHz ultrasound operating at an intensity (in water) of 365 W cm^{-2} ($p_+ = 4$ MPa, $p_- = 3$ MPa), which appears qualitatively very similar to water atomization at similar intensities. The jets explode in a triangular pattern at velocities reaching 10.2 m s^{-1}. These initial atomization events excite further atomization events as shown in the final frame. This figure is available in video format in supplementary movie 2.

static pressure increases to 1.39 MPa, there is a significant reduction in the number of emitted droplets and the fountain drop-chain structure becomes more definite. Droplets are released at slower velocities ranging from 2 to 5 m s^{-1}, with diameters ranging from 50 to 200 μm. The drop-chain fountain remains as the static pressure increases to 2.41 and 3.45 MPa, with fewer droplets of similar size and velocity emitted as the pressure increases. Once the pressure reaches 6.89 MPa, no droplets are emitted. This trend continues as the pressure increases to 8.27 and 10.34 MPa. Interestingly, however, when the static pressure reaches 13.79 MPa, a few droplets are again emitted. These droplets range between 100 and 200 μm in diameter and are emitted at even slower velocities of less than 2 m s^{-1}.

When the acoustic intensity is increased to 1200 W cm^{-2} ($p_+ = 6.8$ MPa, $p_- = 5.3$ MPa), atomization is even more dramatic at atmospheric pressure with droplet diameters ranging from less than 20 μm (1 pixel) to 550 μm emitted at velocities up to 11 m s^{-1} as shown in figure 10. As before, the drop-chain structure begins to become more defined at 1.38 MPa, and a few droplets of 40–300 μm in diameter are released from the drop chain at velocities up to 7.5 m s^{-1} for each static pressure level up to 3.45 MPa; the number of emitted droplets decreases with increasing static pressure (to keep the timing similar between frames in the figure, not all pressure levels show the release of droplets). Even fewer droplets are released when the static pressure reaches 6.89 and 8.27 MPa; however, when the static pressure reaches 10.34

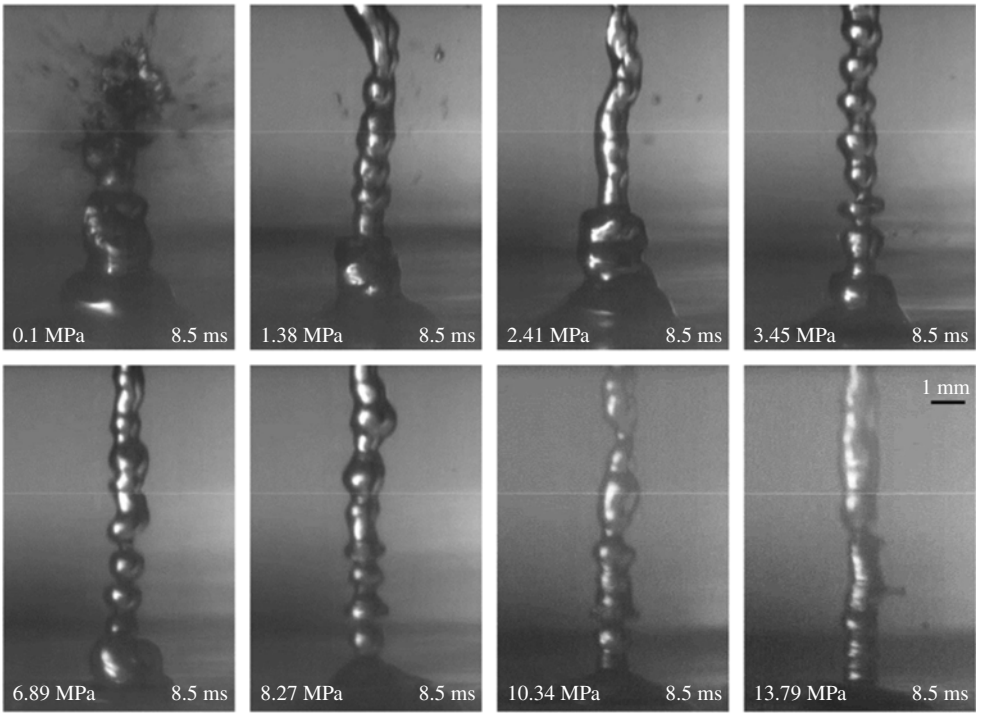

FIGURE 9. Water atomization in the overpressure chamber from the 2.127 MHz focused ultrasound transducer operating at 850 W cm^{-2} ($p_+ = 5.5$ MPa, $p_- = 4.5$ MPa) and recorded at 10 000 f.p.s. At atmospheric pressure (0.1 MPa), atomization is very dramatic, with droplets ranging from less than 20 (1 pixel) up to 400 μm in diameter and emitted at velocities ranging from 2 to 8 m s^{-1}. When the static pressure applied to the system reaches 1.38, 2.41 and 3.45 MPa, the fountain becomes drop-chain in structure and a decreasing number of droplets are emitted. As the pressure is increased to 6.89, 8.27, or 10.34 MPa, atomization ceases and no droplets are emitted during the 10 ms exposures. Interestingly, however, when the static pressure increases still further to 13.79 MPa, droplets are again released from the drop chain. Select static pressure levels from this figure are available in video format in supplementary movie 3.

or 13.79 MPa, the number of emitted droplets increases. These droplets are uniformly large (between 100 and 400 μm in diameter) and released at very slow velocities of 1–2 m s^{-1}. When the static pressure is returned to atmospheric levels, atomization again proceeds very similarly to what was originally observed at atmospheric pressure (not shown).

4. Discussion

This paper presents a series of experimental results that show the key role of bubbles in the atomization of the drop-chain fountain. Moreover, in addition to the existing explanation of the bubbles' role in atomization in the form of acoustic cavitation, the novel idea has been proposed that boiling is a viable mechanism contributing to atomization in the drop-chain fountain under some regimes.

When the ultrasonic frequency and liquid speed of sound were varied, it was found that, at least for transducers with an F-number of one, the diameter of the drop-chain

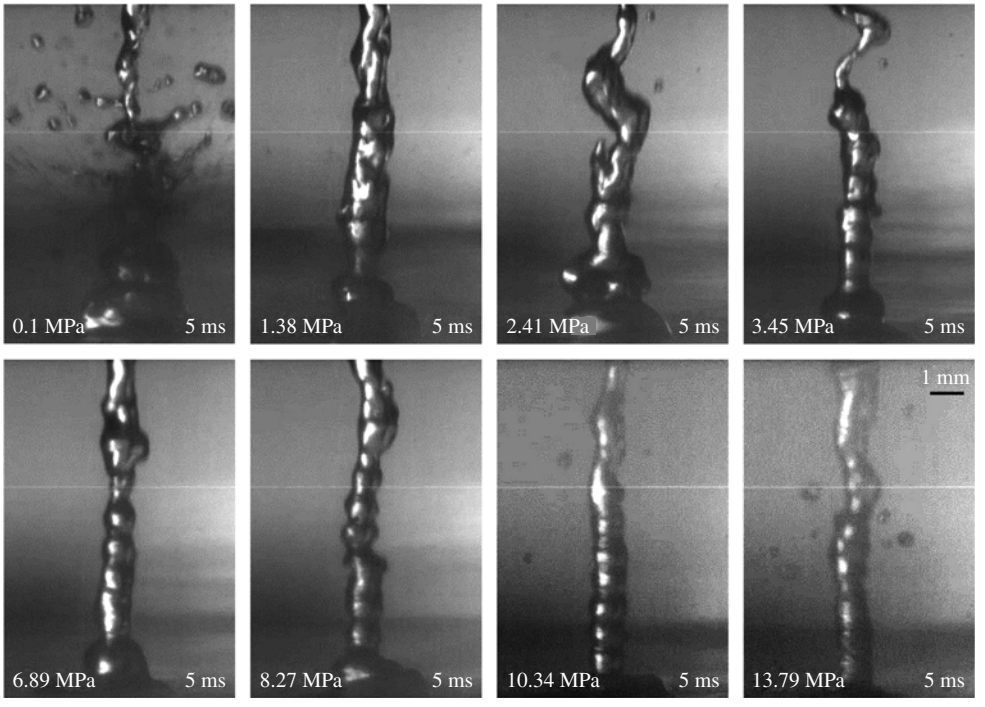

FIGURE 10. Water atomization from the 2.127 MHz focused ultrasound transducer operating at 1200 W cm^{-2} ($p_+ = 6.8, p_- = 5.3$ MPa) and recorded at 10 000 f.p.s. for a range of static pressure levels. At 0.1 MPa, atomization is dramatic, with droplet diameters ranging from less than 20 (1 pixel) up to 550 μm in diameter and jet velocities reaching 11 m s^{-1}. When the static pressure is increased to 1.38, 2.41, or 3.45 MPa, atomized droplets are larger and released at slower velocities ranging up to 7.5 m s^{-1}. When the static pressure is increased to 6.89 or 8.27 MPa, very few droplets are emitted in the 10 ms pulse (not shown); however when the static pressure is increased to 10.34 or 13.79 MPa, droplets of diameters between 100 and 400 μm are released at velocities of 1–2 m s^{-1}. Select static pressure levels are available in video format in supplementary movie 4.

approximately equals the acoustic wavelength. This effect can be due to two reasons. First, the acoustic radiation force forms the hydrodynamic jet on the liquid surface, and thus this jet has a diameter that approximately coincides with the acoustic beam width, which is defined by the diffraction effect. The ultrasound intensity of a uniformly vibrating, curved (focused) source has the following distribution at the focal plane (O'Neil 1949):

$$I = I_0 \left(\frac{2\mathrm{J}_1(\xi)}{\xi} \right)^2, \tag{4.1}$$

where I_0 is the focal intensity, $\mathrm{J}_1(\xi)$ is the Bessel function of the first kind, $\xi = \pi x/(\lambda F)$, x is the transverse coordinate, λ is the wavelength, and F is the F-number (ratio of the focal distance to the source diameter). From this, the beam diameter D, as defined by the half-intensity level, can be approximately expressed as $D \approx 1.03\lambda F$, i.e. for the experimental situation of the F-number equal to one, the beam width coincides with the wavelength. As the drop chain is formed from the emitted fountain jet, each

drop diameter is on the order of λ. The second reason for the diameter of the drops to be very close to a wavelength is due to the fact that the acoustic radiation force enhancement (that is needed for the drop to be effectively pushed) happens when the acoustic energy density at the liquid surface is increased, i.e. the incident wave is effectively trapped by the up-going protuberance on the water surface. This occurs when the drop growing from that protuberance becomes an efficient acoustic absorber, which, in turn, happens when the resonance frequency of the drop becomes close to the incident wave frequency. A spherical standing wave inside a spherical drop is expressed as

$$p = p_0 \frac{\sin(2\pi r/\lambda)}{2\pi r/\lambda}, \tag{4.2}$$

where p_0 is the acoustic pressure amplitude at the drop centre and r is the distance from that centre. At the drop surface, $r = R$, the acoustic pressure is released, which gives the condition for the possible resonance radii $R_n = n\lambda/2$, where $n = 1, 2, \ldots$. From this, the lowest resonance corresponds to the drop diameter $d = 2R_1$ which equals one wavelength.

Across the tested frequencies, a qualitative similarity in atomization was observed in that a distortion in the top drop was observed immediately before jets were emitted. These distortions appear similar to the chaotic oscillations that are often observed in vibrated bubbles shortly before jetting (Movassat 2012). In the 1.04 MHz atomization video (figure 4*a*), it was noted that the top drop in the chain changes from transparent to opaque immediately before atomization, which would suggest that some sort of surface instability, such as capillary waves, contributes to atomization. However, observations by Shepherd (1981) of superheated butane drops showed similar changes in drop opacity immediately before the explosion occurred due to boiling. Moreover, in some cases (e.g. figure 5) drops remained transparent and an opacity within the drop, which we speculated were cavitation or boiling bubbles, preceded the explosion. Additionally, as the frequency decreased, the time to commence atomization increased, though the number of cycles to commence atomization was similar across the tested frequencies. This result suggests that atomization arises from a cumulative process such as capillary waves or boiling.

When water was exchanged for liquids with various shear viscosities, it was found that, in general, the atomization threshold increased with the shear viscosity, even when accounting for the differences in the absorption coefficients between liquids. This observation can be explained by the fact that the larger viscosity corresponds to higher absorption for the standing spherical wave, which reduces the acoustic pressure level in the centre of the drop and thus increases the cavitation threshold and reduces heating of the drop centre. On the other hand, shear viscosity also damps surface instabilities. When the water temperature was increased, the time to commence atomization decreased. While heating influences the surface tension, cavitation threshold, and time to boil, results from Crum (1979) show a strong effect of temperature on the cavitation threshold whereas the dependence of temperature on surface tension is very small. Thus, these temperature dependences, and the decrease in the time to commence atomization with increasing temperature, as well as the strong influence of shear viscosity on the atomization threshold, suggest that bubbles, either through acoustic cavitation or boiling, play a greater role than capillary waves in the atomization of the drop-chain fountain.

Note that liquid viscosity and surface tension influence not only atomization, but also the formation of the drop-chain fountain, which can be considered a result of fountain or jet instability. Tomotika (1935, 1936) has shown that an incompressible

cylindrical jet becomes unstable at a characteristic time τ that is related to the jet diameter D and the liquid parameters as $\tau \approx D\rho_0\eta/\sigma$, where ρ_0 is the density, η is the coefficient of shear viscosity, and σ is the surface tension of the liquid. Although this relationship was obtained for a different type of jet, it can be used to understand the influence of viscosity and surface tension on how rapidly the jet is broken into a drop-chain fountain. From the parameters given in table 1, it follows that the most unstable (smallest τ) is the water jet, with the slowest instability being developed in castor oil (approximately 2200 times slower). The latter fact could explain why drop formation was never observed in the castor oil fountain.

The final study, where atomization was explored in an overpressure chamber, was designed to isolate surface instabilities from bubbles in atomization. In the overpressure experiments, the initial results showed that atomization was reduced or completely suppressed as the static pressure increased, leading to the conclusion that bubbles cause atomization in the drop-chain fountain. However when the static pressure was increased even further, droplets were again released from the drop-chain fountain. While supporting that suppression of bubbles has a significant effect, it is counterintuitive that at higher static pressures atomization (in a diminished state) returns. One possible explanation is in the drop-chain structure. At 13.79 MPa, the drop chain is less consistent in definition; at times, the fountain sides appear smooth and droplets are released when the fountain transitions between smooth and drop-chain sides, perhaps in a breathing-mode ejection of fluid mass. These transitions in and out of the drop-chain structure could be due to the difference in the interactions between reflected waves and incoming waves within the water column caused by the changes in the speed of sound of water or changes in the acoustic impedance of air. At 13.79 MPa, according to Medwin (1975) only a slight increase in the speed of sound of approximately 62 m s^{-1} would be expected. However, there is also an increase in the characteristic impedance in air of approximately 56 kRayleighs at 13.79 MPa compared to atmospheric pressure. The increases in the impedance of both air and water when the static pressure is 13.79 MPa cause an increase in the intensity transmission and reflection coefficients on the order of 100; at 13.79 MPa, the intensity transmission coefficient (normal incidence) is 0.14 as compared to 0.001 at atmospheric pressure. The intensity transmission coefficient shows how efficiently acoustic energy is leaving the water surface or the drops in the chain. It is possible that the changes in the impedances with increasing static pressure influence the wave interactions in such a way that causes the droplets to be released at 13.79 MPa when atomization had completely ceased at 6.89 MPa. Modelling of the acoustic wave in the fountain could help explain this phenomenon.

In the observed phenomenon of atomization, it is hard to separate the effect of acoustically driven gas bubbles (acoustic cavitation) from thermally driven vapour bubbles (boiling). Indeed, both types of bubbles are affected by the static pressure and temperature changes in a similar way. The possible role of acoustic cavitation was proposed earlier (Sollner 1936; Rozenberg & Eknadiosyants 1960; Gershenzon & Eknadiosyants 1964; Il'in & Eknadiosyants 1967, 1969); however, in the wide range of acoustic parameters (frequency and intensity), types of liquids, and ambient conditions (static pressure and temperature) that were used, indications of the appearance of boiling have been observed. Bear in mind that boiling in a superheated drop, if it happens, should have the form of an explosion. Observations of thin jets that are sometimes emitted from the drop surface (see e.g. photos in figures 4, 5 and 8) are more likely to be due to the explosion of a vapour bubble in the superheated part of the drop, supposedly near the drop centre.

Note that the drops in the chain could be fairly efficient energy concentrators, because the acoustic wave that penetrates into a drop through a thin waist on its bottom is effectively trapped inside the drop. For instance, consider a case that corresponds to figure 4(*a*). Suppose that the acoustic intensity of $I = 245$ W cm^{-2} is acting on the acoustic fountain consisting of two drops at $\tau = 4$ ms. The corresponding amount of acoustic energy that is trapped by the drops can be estimated as $I\tau\pi d^2/4$, where $d = 1.5$ mm, the drop diameter. Supposing this energy is evenly divided between two drops (see figure 4*a*), the energy trapped in the upper drop can be estimated as $E = 0.01$ J. In reality, some amount of energy of the focused ultrasound beam will be reflected back towards the transducer, but this should not change the estimate too much. The acoustic pressure amplitude inside the drop is distributed according to (4.2). It can be shown that the total acoustic energy of a drop of one wavelength diameter and the pressure amplitude at its centre are related by the following expression:

$$E \approx \frac{d^3}{8\pi}\frac{p_0^2}{\rho_0 c_0^2}, \tag{4.3}$$

where ρ_0 is the liquid density, and c_0 is the sound velocity. From this it follows that for a drop of water, $E = 0.01$ J corresponds to $p_0 \approx 400$ MPa. Even if the estimated value for the drop energy is significantly reduced, the predicted maximum pressure is still very high: for $E = 0.001$ J, it is 130 MPa, and for even smaller energy $E = 0.0001$ J, it is 40 MPa. This indicates that the acoustic pressure in the centre of the drop could be so high that the acoustic cavitation threshold could be easily reached.

At such high pressures, boiling can also be achieved. If the temperature were uniform inside the drop, it would be increased by

$$\Delta T = \frac{E}{\rho_0 c_p V}, \tag{4.4}$$

where $\rho_0 = 1000$ kg m^{-3} is the density of water, $c_p = 4200$ J kg^{-1} K^{-1} is the specific heat, and $V = \pi d^3/6$ is the drop volume. The estimate gives $\Delta T \approx 1.3$ K which is much below the increase needed for boiling. Therefore, the uniformly heated drop would not reach boiling temperature. This was confirmed in an additional experiment (not presented here) with a high-speed infrared camera that showed that the drop surface was indeed not heated by more than 1 K. However, the above assumption of uniform temperature distribution is too simplified. Even in the linear regime, the drop is heated by a standing wave (4.2), i.e. non-uniformly. At 100 MPa pressure levels, the standing wave inside the drop behaves nonlinearly and thus is being more efficiently absorbed in the central part of the drop, especially if shock fronts are generated in the pressure waveform. Theoretical analysis accounting for medium nonlinearity is needed to calculate the corresponding drop heating: this challenging task is outside the scope of the current study.

Atomization in a drop-chain fountain has been of interest since atomization was first discovered in 1927. In this paper, it is shown: that the ultrasound excitation frequency and liquid speed of sound affect the drop-chain diameter; the time to commence atomization decreases when the temperature increases; the threshold for atomization increases with shear viscosity; and atomization is significantly diminished by overpressure. A limitation of this study was that no test changed only one mechanism of interest. For example, changing the shear viscosity also changed the surface tension and increasing the water temperature influenced the boiling, acoustic

cavitation, and surface wave mechanisms. Nevertheless, these results show the key role of bubbles in the atomization of the drop-chain fountain, and experimental observations and calculations suggest that these bubbles could arise from acoustic cavitation or boiling. More research and extensive modelling may be able to further elucidate the origin of the bubbles, although it is possible that atomization in the drop-chain fountain is complex enough to be caused by a combination of acoustic cavitation, boiling, and even surface instabilities, depending on the exact geometry and physical properties of the chain.

Acknowledgements

This work was supported by the National Institute of Health (DK043881 and EB007643), the Russian Foundation for Basic Research (13-02-00183 and 14-02-00426), and the National Space Biomedical Research Institute in consortium agreement with the National Aeronautics and Space Administration NCC 9-58. The authors gratefully acknowledge the help of Dr T. Khokhlova and Dr W. Kreider for fruitful discussions and B. MacConaghy for building and testing the overpressure chamber. The authors also wish to thank the staff and researchers at the Center for Industrial and Medical Ultrasound (CIMU).

Supplementary movies

Supplementary movies are available at http://dx.doi.org/10.1017/jfm.2015.11.

REFERENCES

ANTONEVICH, J. N. 1959 Ultrasonic atomization of liquids. *Ultrason. Engng: Trans. IRE Professional Group* **6**, 6–15.

BAILEY, M. R., COURET, L. N., SAPOZHNIKOV, O. A., KHOKHLOVA, V. A., TER HAAR, G., VAEZY, S., SHU, X. & CRUM, L. A. 2001 Use of overpressure to assess the role of bubbles in focused ultrasound lesion shape *in vitro*. *Ultrasound Med. Biol.* **27**, 695–708.

BARRERAS, F., AMAVEDA, H. & LOZANO, A. 2002 Transient high-frequency ultrasonic water atomization. *Exp. Fluids* **33**, 405–413.

BASSETT, J. D. & BRIGHT, A. W. 1976 Observations concerning the mechanism of atomisation in an ultrasonic fountain. *J. Aero. Sci.* **7**, 47–51.

BLAMEY, J., YEO, L. L. & FRIEND, J. R. 2013 Microscale capillary wave turbulence excited by high frequency vibration. *Langmuir* **29**, 3835–3845.

BOGUSLAVSKII, Y. Y. & EKNADIOSYANTS, O. K. 1969 Physical mechanism of the acoustic atomization of a liquid. *Sov. Phys. Acoust.* **15**, 14–21.

BRONSKAYA, L. M., VIGDERMAN, V. S., SOKOL'SKAYA, A. V. & EL'PINER, I. E. 1968 Influence of the static pressure on ultrasonic chemical and biological effects. *Sov. Phys. Acoust.* **13**, 374–375.

COLLINS, D. J., MANOR, O., WINKLER, A., SCHMIDT, H., FRIEND, J. R. & YEO, L. L. 2012 Atomization off thin water films generated by high-frequency substrate wave vibrations. *Phys. Rev.* E **86**, 056312.

CRUM, L. A. 1979 Tensile strength of water. *Nature* **278**, 148–149.

EKNADIOSYANTS, O. K. 1968 Role of cavitation in the process of liquid atomization in an ultrasonic fountain. *Sov. Phys. Acoust.* **14**, 80–84.

GERSHENZON, E. L. & EKNADIOSYANTS, O. K. 1964 The nature of liquid atomization in an ultrasonic fountain. *Sov. Phys. Acoust.* **10**, 127–132.

HILL, C. R. 1971 Ultrasonic exposure thresholds for changes in cells and tissues. *J. Acoust. Soc. Am.* **51**, 667–672.

IL'IN, B. I. & EKNADIOSYANTS, O. K. 1967 Nature of the atomization of liquids in an ultrasonic fountain. *Sov. Phys. Acoust.* **12**, 269–275.

IL'IN, B. I. & EKNADIOSYANTS, O. K. 1969 Influence of static pressure on the utlrasonic fountain effect in a liquid. *Sov. Phys. Acoust.* **14**, 452–455.

KHOKHLOVA, V. A., BAILEY, M. R., REED, J. A., CUNITZ, B. W., KACZKOWSKI, P. J. & CRUM, L. A. 2006 Effects of nonlinear propagation, cavitation, and boiling in lesion formation by high intensity focused ultrasound in a gel phantom. *J. Acoust. Soc. Am.* **119**, 1834–1848.

KUJAWSKA, T. 2012 Pulsed focused nonlinear acoustic fields from clinically relevant therapeutic sources in layered media: experimental data and numerical prediction results. *Arch. Acoust.* **37**, 269–278.

LANG, R. J. 1962 Ultrasonic atomization of liquids. *J. Acoust. Soc. Am.* **34**, 6–8.

MAXWELL, A. D., CAIN, C. C., HALL, T. L., FOWLKES, J. B. & XU, Z. 2013 Probability of cavitation for single ultrasound pulses applied to tissues and tissue-mimicking materials. *Ultrasound Med. Biol.* **39**, 449–465.

MCCUBBIN, J. K. JR 1953 The particle size distribution in fog produced by ultrasonic radiation. *J. Acoust. Soc. Am.* **25**, 1013–1014.

MEDWIN, H. 1975 Sound speed in water: a simple equation for realistic parameters. *J. Acoust. Soc. Am.* **58**, 1318–1319.

MOVASSAT, M. 2012 Bubble dynamics, oscillations and breakup under forced vibration. PhD thesis, University of Toronto.

National Physical Laboratories 2013 Table of physical and chemical constants. URL: http://kayelaby.npl.co.uk.

O'NEIL, H. T. 1949 Theory of focusing radiators. *J. Acoust. Soc. Am.* **121**, 516–526.

QI, A., YEO, L. Y. & FRIEND, J. R. 2008 Interfacial destabilization and atomization driven by surface acoustic waves. *Phys. Fluids* **20**, 074103.

ROZENBERG, L. D. & EKNADIOSYANTS, O. K. 1960 Kinetics of ultrasonic fog formation. *Sov. Phys. Acoust.* **6**, 369–374.

ROZENBERG, L. D. (Ed.) 1973 *Physical Principles of Ultrasonic Technology,* vol. 2. Plenum.

SAPOZHNIKOV, O. A., KHOKHLOVA, V. A., BAILEY, M. R., WILLIAMS, J. C., MCATEER, J. A., CLEVELAND, R. O. & CRUM, L. A. 2002 Effect of overpressure and pulse repetition frequency on cavitation in shock wave lithotripsy. *J. Acoust. Soc. Am.* **112**, 1183–1195.

SHEPHERD, J. E. 1981 Dynamics of vapor explosions: rapid evaporation and instability of butane droplets exploding at the superheat limit. PhD thesis, California Institute of Technology.

SIMON, J. C., SAPOZHNIKOV, O. A., KHOKHLOVA, V. A., WANG, Y.-N., CRUM, L. A. & BAILEY, M. R. 2012 Ultrasonic atomization of tissue and its role in tissue fractionation by high intensity focused ultrasound. *Phys. Med. Biol.* **57**, 8061–8078.

SOLLNER, B. Y. K. 1936 The mechanism of the formation of fogs by ultrasonic waves. *Trans. Faraday Soc.* **32**, 1532–1536.

The Engineering Toolbox 2013 URL: http://www.engineeringtoolbox.com.

TOMITA, Y. & TANAKA, S. 2012 Focused ultrasound induced free-surface breakup and damage in acrylic plates. *AIP Conf. Proc.* **1474**, 123–126.

TOMOTIKA, S. 1935 On the instability of a cylindrical thread of a viscous liquid surrounded by another viscous fluid. *Proc. R. Soc. Lond.* A **150**, 322–337.

TOMOTIKA, S. 1936 Breaking up of a drop of viscous liquid immersed in another viscous fluid which is extending at a uniform rate. *Proc. R. Soc. Lond.* A **153**, 302–318.

TOPP, M. N. 1973 Ultrasonic atomization – a photographic study of the mechanism of disintegration. *Aero. Sci.* **4**, 17–25.

TREEBY, B. E., COX, B. T., ZHANG, E. Z., PATCH, S. K. & BEARD, P. C. 2009 Measurement of broadband temperature-dependent ultrasonic attenuation and dispersion using photoacoustics. *IEEE Trans. Ultrason. Ferroelectr. Freq. Control* **56**, 1666–1676.

WOOD, R. W. & LOOMIS, A. L. 1927 Physical and biological effects of high-frequency sound-waves of great intensity. *Phil. Mag.* **4**, 417–436.